A Quantum Wave Packet Dynamical Study of the Electronic and Spin−Orbit Coupling Effects on the Resonances in $Cl(^2P) + H_2$ Scattering

Subhas Ghosal and Susanta Mahapatra*

School of Chemistry, University of Hyderabad, Hyderabad 500 046, India

Received: November 3, 2004; In Final Form: December 7, 2004

Dynamical resonances in $Cl(^2P) + H_2$ scattering are investigated with the aid of a time-dependent wave packet approach using the Capecchi−Werner coupled ab initio potential energy surfaces [*Phys. Chem. Chem. Phys.* **2004**, *6*, 4975]. The resonances arising from the prereactive van der Waals well (∼0.5 kcal/mol) and the transition-state (TS) region of the $^2\Sigma_{1/2}$ ground spin−orbit (SO) state of the $Cl(^2P) + H_2$ system are calculated and assigned by computing their eigenfunctions and lifetimes. The excitation of even quanta along the bending coordinate of the resonances is observed. The resonances exhibit an extended van der Waals progression, which can be attributed to the dissociative states of ClH_2. Excitation of H_2 vibration is also identified in the high-energy resonances. The effect of the excited $^2P_{1/2}$ SO state of Cl on these resonances is examined by considering the electronic and SO coupling in the dynamical simulations. While the electronic coupling has only a minor impact on the resonance structures, the SO coupling has significant effect on them. The nonadiabatic effect due to the SO coupling is stronger, and as a result, the spectrum becomes broad and diffuse particularly at high energies. We also report the photodetachment spectrum of ClD_2^- and compare the theoretical findings with the available experimental results.

I. Introduction

The simplest Cl atom reaction, $Cl + H_2 \rightarrow HCl + H$ has been a classic example for the basic understanding of chemical reaction dynamics.[1] This reaction has been a subject of research for over a century and served as a prototypical model for the bimolecular reaction rate theory, particularly the transition-state theory ,and a textbook example of the theory of kinetic isotopic effects.[2] Despite a large number of theoretical[3−13] and experimental[14−18] studies on this system, it has drawn renewed attention in recent years because of the realization that the nonadiabatic interactions of different spin−orbit (SO) states of the Cl atom can play a significant role on its reaction dynamics in the ground SO state. The reactivity of the excited SO state of Cl and the existence of a van der Waals well (∼0.5 kcal/mol) in the reagent asymptote and its influence on the reaction dynamics are the two most important issues addressed in the current literature.[4,5,14,15]

The approach of the closed shell H_2 molecule to the Cl atom splits the threefold degeneracy of the ^2P state and leads to three adiabatic electronic states with $^2\Sigma_{1/2}$, $^2\Pi_{3/2}$, and $^2\Pi_{1/2}$ symmetries in collinear geometries ($1\ ^2A'$, $1\ ^2A''$, and $2\ ^2A'$ symmetries, respectively, in noncollinear geometries). This splitting has been schematically shown in Figure 1. In this figure, the adiabatic potential energies of the SO states of the $Cl(^2P) + H_2$ system are plotted along the collinear reaction path. In reagent arrangement, the first two states correlate to the ground $^2P_{3/2}$ SO state of the atomic Cl, and the third state correlates to its excited $^2P_{1/2}$ SO state. The two states of $^2A'$ symmetry are electronically coupled at the linear geometry and form a conical intersection (see Figures 4 and 5 of ref 10). In the product arrangement, the $^2\Sigma_{1/2}$ adiabatic state correlates with the electronic ground state of the products $HCl\ (X^1\Sigma^+) + H\ (^2S)$, whereas the other two states (the components of the $^2\Pi$ state) correlate with the products in the electronic excited state, $HCl\ (^3\Pi) + H(^2S)$.[3−5,8] The latter two states are adiabatically closed at low and moderate collision energies. They can yield products in their electronic ground state via nonadiabatic transitions (Born−Oppenheimer-forbidden) to the $^2\Sigma_{1/2}$ electronic state only.

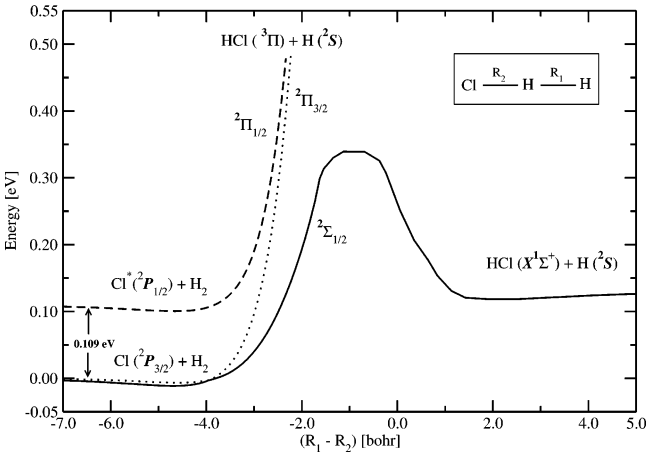

Figure 1. Schematic representation of the adiabatic potential energy surfaces[10] of the $Cl(^2P) + H_2$ system for the collinear arrangements of the three nuclei. Shown are the two SO states and their energetic splitting of ∼0.109 eV. The reagent and product asymptotes (see text) are also marked in the figure. The curves are labeled by the Hund's Case (a). The minimum of the van der Waals well in the reagent asymptote occurs at the T-shaped arrangement of the nuclei.

Over the past few decades, considerable progress has been made toward construction of a global potential energy surface (PES) of the electronic ground state of the $Cl + H_2$ system.[6−8] Despite good success of the semiempirical G3 surface[7] in describing the $Cl + H_2$ reaction dynamics, it revealed striking disagreement with the recent crossed molecular beam results

* E-mail: smsc@uohyd.ernet.in. Fax: +91-40-23012460.

10.1021/jp044972v CCC: $30.25
Published on Web 01/28/2005

on the Cl + HD → HCl(DCl) + H(D) reaction.[3] It failed to reproduce the strong propensity for the DCl product observed in the experiment.[3] In addition, the rotational excitation of the reagent H_2 has been found to hinder the reaction in contrast to the experimental results.[3] Bian and Werner (BW) have developed a three-dimensional ab initio PES,[8] and subsequent quantum scattering calculations on this surface are found to yield a DCl/HCl product branching ratio in agreement with the experiment.[3] The discrepancies between the scattering results on the G3[7] and the BW PESs[8] revealed the importance of the long-range van der Waals forces in the entrance valley of the reaction.[3] Most recently, Capecchi and Werner (CW) extended the BW surface by including the relativistic SO coupling effects.[4,5,10] These authors have developed multiparameter global fits to the resulting six PESs: three diabatic PESs, one electronic coupling surface, and two SO coupling surfaces.[10] With the availability of these multisheeted PESs and their electronic and SO coupling surfaces, more challenging multistate quantum dynamical studies to complement the new experimental results have become possible in recent years.[19]

In our earlier studies, we used the CW PESs and investigated the electronic and SO coupling effects in the reactive scattering dynamics of Cl + H_2 with the aid of the quantum flux operator and a time-dependent wave packet (WP) approach.[11] Using the latter approach, we also calculated the photoelectron spectrum of ClH_2^- for a transition to the coupled manifold of the multisheeted PESs of ClH_2.[12] The theoretical results are found to be in very good accord with the experimental recording of Neumark and co-workers.[16] A Franck−Condon (FC) simulation of this photoelectron spectrum using the same PESs (without considering the coupling surfaces) appeared recently.[20] The photodetachment of ClH_2^- probes the van der Waals well region of the reagent Cl + H_2 asymptote. The theoretical results[12,20] along with the experimental observations[16] provide direct evidence (for the first time) of the importance of the van der Waals well in the reagent asymptote of a chemical reaction. This also, in turn, reveals the spectroscopic accuracy of the CW coupled PESs, which are much more complex to calculate. The quantum scattering results revealed the overall agreement with other theoretical calculations that appeared in the literature.[4,5]

The reactivity of the ground SO state (Cl($^2P_{3/2}$)) is higher than that of the SO excited state (Cl*($^2P_{1/2}$)),[4,5,11] in apparent contradiction to the experimental results.[14,15] The $^2\Pi_{3/2}$ and $^2\Pi_{1/2}$ states lead to the ground-state product via nonadiabatic transitions to the $^2\Sigma_{1/2}$ state. We found that the Σ−Π electronic coupling has only a minor effect on the reactivity of the $^2\Sigma_{1/2}$ state; however, the relativistic SO coupling has a much greater role in it.[11] Both the electronic and SO coupling have much stronger effects on the nuclear dynamics of the $^2\Pi_{3/2}$ and $^2\Pi_{1/2}$ electronic states.

In this article, we set out to investigate the dynamical resonances in the Cl + H_2 system. Our previous theoretical analysis on the ClH_2^- photoelectron spectrum[12] revealed polyad structures at higher-energy resolution. These structures transform to broad bands when viewed at the energy resolution of the photoelectron experiment. Resonances originating from the van der Waals region of the PESs reveal extended progression along the Cl···H_2 van der Waals coordinate. Even quantum excitation along the bending coordinate is observed. The excitation of the H_2 vibration is observed only at high energies. In addition, we also examined the resonances arising from the TS region of the $^2\Sigma_{1/2}$ PES of ClH_2. The impact of the electronic and SO coupling on these resonances is examined and discussed. We also calculate the photodetachment spectrum of ClD_2^- and compare with the experimental results.

Our theoretical approach is based on a time-dependent WP method adapted to simulate the nuclear dynamics on the coupled manifold of three electronic states. The calculations are carried out for the lowest value of the total angular momentum. The pseudospectra are calculated by locating an initial WP at two different regions (van der Waals well as well as the barrier) of the PESs. The resonances are identified from the peaks that appeared in the pseudospectra. The genuineness of different peaks in the pseudospectrum is confirmed by varying the initial location of the WP in the mentioned regions of the PES. Spectra are calculated both for the uncoupled adiabatic and the diabatic states and are compared. The energy eigenvalue and the line width lifetime (whenever possible) are determined by fitting the spectral peaks to a line shape function. The eigenvectors of the resonances are computed by the spectral quantization algorithm. In the coupled-state picture, the dynamics is studied throughout in a diabatic representation, and the impact of the electronic and SO coupling on the dynamical resonances is explicitly examined.

The rest of this paper is organized as follows: Section II contains a brief review of the theoretical approach used. In section III, the results are presented and discussed. The photodetachment spectrum of ClD_2^- is also presented in this section and compared with the experiment. A summary of the findings is given in section IV.

II. Calculation of Resonances by a Time-Dependent Wave Packet Approach

In this section, we describe the calculation of resonances by a time-dependent WP approach.[21] Because such an approach has become a standard tool in the literature, we will discuss only the essentials here, particularly focusing on the nuclear dynamics of the coupled multisheeted electronic states. In the time-dependent WP, approach the pseudospectrum pertinent to an FC transition of a hypothetical initial state to the final coupled manifold of three electronic states of the Cl(^{2}P) + H_2 system is calculated. The spectral intensity is given by the time-dependent version of the golden rule equation[22]

$$I(E) \approx |\int_0^T e^{iEt/\hbar} C(t)\, dt| \tag{1}$$

The quantity $C(t) = \langle \Psi(t=0)|\Psi(t)\rangle$ in eq 1 is the autocorrelation function of the system at time t. This is calculated by propagating the hypothetical initial state $|\Psi(t=0)\rangle$ on the final coupled manifold of three electronic states in the diabatic electronic representation with the aid of the time-dependent Schrödinger equation (TDSE). For an explicitly time-independent Hamiltonian, the solution of the TDSE reads

$$|\Psi(t)\rangle = \exp\left[-\frac{i\mathscr{H}t}{\hbar}\right]\Psi(t=0) \tag{2}$$

where $|\Psi(t)\rangle$ represents the wave function of the system at time t. The quantity $\mathscr{H}$ represents the 3 × 3 Hamiltonian matrix of the Cl(^{2}P) + H_2 system. This is most conveniently written in a diabatic electronic representation as

$$\mathscr{H} = \mathscr{H}^{Nu}\mathbf{1} + \mathscr{H}^{el} + \mathscr{H}^{so} \tag{3}$$

where $\mathscr{H}^{Nu}$ represents the nuclear kinetic energy part of the Hamiltonian matrix, which is diagonal in this representation. **1** is a 3 × 3 unit matrix. The coupling between the states is described by the off-diagonal elements of the electronic ($\mathscr{H}^{el}$)

plus the relativistic SO ($\mathscr{H}^{SO}$) Hamiltonian matrix. In the following, we describe the elements of this Hamiltonian matrix in terms of the body-fixed Jacobi coordinates R (the distance of the Cl atom from the center-of-mass of H_2), r (the H_2 internuclear distance), and γ (the angle between $\vec{R}$ and $\vec{r}$) of the $Cl + H_2$ arrangement channel. The body-fixed z axis is defined as parallel to $\vec{R}$, and H_2 lies in the xz plane. In terms of these coordinates, $\mathscr{H}^{Nu}$ is given by

$$\mathscr{H}^{nu} = -\frac{\hbar^2}{2\mu}\left[\frac{\partial^2}{\partial R^2} + \frac{\partial^2}{\partial r^2}\right] - \frac{\hbar^2}{2I}\frac{1}{\sin\gamma}\frac{\partial}{\partial\gamma}\left(\sin\gamma\,\frac{\partial}{\partial\gamma}\right) + \frac{(\mathbf{J}^2 + \mathbf{L}^2)}{2\mu R^2} - \frac{(2\mathbf{J}.\mathbf{L} + 2\mathbf{J}.\mathbf{j} - 2\mathbf{j}.\mathbf{L})}{2\mu R^2} \quad (4)$$

where $\mu = [m_{Cl}m_H^2/(m_{Cl} + 2m_H)]^{1/2}$ [23] (m_{Cl} and m_H being the masses of the Cl and H atoms, respectively) is the three-body uniform reduced mass, and $I = \mu R^2 r^2/(R^2 + r^2)$ is the three-body moment of inertia. The first term in eq 4 represents the radial kinetic energy operators along R and r. The various angular momentum terms appearing in eq 4 are denoted following the work of Rebentrost and Lester,[24] Schatz and co-workers,[25] and Alexander and co-workers.[26] The total electronic angular momentum of the atom is denoted by $\mathbf{L}$ ($=\mathbf{l} + \mathbf{s}$; $\mathbf{l}$ and $\mathbf{s}$ being the electronic orbital and spin angular momentum with l and s being the associated quantum numbers, respectively) with L being the corresponding quantum number. The total (electronic + nuclear) angular momentum is denoted by $\mathbf{J}$ with corresponding quantum number J. $\mathbf{j}$ denotes the diatomic rotational angular momentum, with j being the corresponding quantum number. The rotational kinetic energy operator of the diatom $\mathbf{j}^2/2I$, depending on the Jacobi angle γ, is expressed by the second term of eq 4. The rest of eq 4 describes other centrifugal and Coriolis coupling terms. The body-fixed projection quantum numbers associated with $\mathbf{j}$, $\mathbf{L}$, and $\mathbf{J}$ may be denoted as $\Omega_\mathbf{j}$, $\Omega_\mathbf{L}$, and $\Omega_\mathbf{J}$, respectively. With the present choice of the body-fixed z axis, $\Omega_\mathbf{J} = \Omega_\mathbf{j} + \Omega_\mathbf{L}$.

In a diabatic electronic basis, the matrix representation $\mathscr{H}^{el} + \mathscr{H}^{SO}$ is not diagonal. As stated already, the off-diagonal matrix elements describe the various coupling potentials of the electronic states. By following the prescription of Alexander and co-workers,[26] $\mathscr{H}^{el} + \mathscr{H}^{SO}$ for the $^2\Sigma_{1/2}$, $^2\Pi_{3/2}$, and $^2\Pi_{1/2}$ (1A′, 1A″, and 2A′ species, respectively, in the nonlinear geometry) electronic states of ClH_2 can be decoupled into two 3×3 blocks using a complex basis invariant to time reversal. In terms of their diabatic sign$-\lambda$ representation, $\mathscr{H}^{el} + \mathscr{H}^{SO}$ is given by

$$\mathscr{H}^{el} + \mathscr{H}^{so} = \begin{pmatrix} \mathbf{H} & 0 \\ 0 & \mathbf{H}^\dagger \end{pmatrix} \quad (5)$$

where $\mathbf{H}$ is a 3×3 Hermitian matrix

$$\mathbf{H} = \begin{pmatrix} V_\Sigma & -V_1 - i\sqrt{2}B & V_1 \\ -V_1 + i\sqrt{2}B & V_\Pi + A & V_2 \\ V_1 & V_2 & V_\Pi - A \end{pmatrix} \quad (6)$$

where $A = i\langle\Pi_y|\mathscr{H}^{so}|\Pi_x\rangle$ and $B = \langle\bar{\Pi}_x|\mathscr{H}^{so}|\Sigma\rangle$ are the components of the $\Pi-\Pi$ and $\Sigma-\Pi$ coupling Hamiltonian. The elements of this Hamiltonian matrix are provided by the CW PES.[10] We will use this PES in the text to follow in the calculations of the $Cl + H_2$ resonances.

The initial wave function of the system can be written in a vector notation as

$$|\Psi(R, r, \gamma, t = 0)\rangle = \Psi_1(R, r, \gamma)\begin{pmatrix}1\\0\\0\end{pmatrix} + \Psi_2(R, r, \gamma)\begin{pmatrix}0\\1\\0\end{pmatrix} + \Psi_3(R, r, \gamma)\begin{pmatrix}0\\0\\1\end{pmatrix}, \quad (7)$$

where

$$\begin{pmatrix}1\\0\\0\end{pmatrix},$$

$$\begin{pmatrix}0\\1\\0\end{pmatrix},$$

and

$$\begin{pmatrix}0\\0\\1\end{pmatrix}$$

denotes the $^2\Sigma_{1/2}$, $^2\Pi_{3/2}$, and $^2\Pi_{1/2}$ diabatic electronic states, respectively. The function Ψ_i ($i = 1, 2, 3$) is the nuclear wave function in the respective electronic state depending on the set of Jacobi coordinates introduced already. This wave function is chosen as a stationary Gaussian wave packet (GWP)

$$|\Psi_i(R, r, \gamma)\rangle = N\exp\left[-\frac{(R - R^0)^2}{2\sigma_R^2} - \frac{(r - r^0)^2}{2\sigma_r^2}\right] \times \left\{\exp\left[-\frac{(\gamma - \gamma^0)^2}{2\sigma_\gamma^2}\right] + \exp\left[-\frac{(\gamma - \pi + \gamma^0)^2}{2\sigma_\gamma^2}\right]\right\}, \quad (8)$$

initially located at R^0, r^0, and γ^0 on the respective PES. The quantity N is the normalization constant, and the width parameters of the GWP along R, r, and γ are defined by σ_R, σ_r, and σ_γ, respectively. These initial parameters are suitably varied in order to selectively choose the average energy of the GWP and to map out all the quasi-bound states corresponding to resonances in a given energy window with appreciable intensity.

Once this initial wave function is prepared, it is propagated in the coupled manifold of final electronic states in a diabatic representation with the aid of eq 2. The diabatic electronic representation is chosen in order to avoid the singular behavior of the nonadiabatic coupling terms of the adiabatic electronic representation at or near the vicinity of the seam of the intersections of the PESs.[27] The TDSE (eq 2) is numerically solved on a grid consisting of equally spaced points along the Jacobi distances R and r. The grid along γ is chosen as the nodes of an n-point Gauss$-$Legendre quadrature (GLQ).[28] A 128×64 grid is used in the R and r plane with $0.1a_0 \le R \le 14.197a_0$ and $0.1a_0 \le r \le 8.101a_0$. The grid along the Jacobi angle γ is chosen as the nodes of a 49-point GLQ. The calculations are carried out for the lowest value of the partial wave contributions ($\mathbf{J} = 0$ in the nonrelativistic case and $\mathbf{J} = 0.5$ in the relativistic case). We note that the Coriolis coupling terms of the Hamiltonian in eq 4 are not included in our calculations.

The exponential time evolution operator in eq 4 is evaluated by dividing the time axis into N segments of length Δt each. The exponential operator at each time step is then approximated by the split-operator method of Feit and Fleck,[29] which is adapted to the present coupled-state problem as discussed in

the literature.[11,12,30−32] The fast Fourier transform method[33] and the discrete variable representation[34] method are used to evaluate the action of the radial and angular kinetic energy operators on the wave function, respectively. The WP is time-propagated with a time step $\Delta t \approx 0.135$ fs for a total time of $\sim$2.2 ps. Because in the following applications, we start from a real initial wave function, we utilize the prescription to calculate $C(2t) = \langle\Psi(t)^*|\Psi(t)\rangle$, which allows us to increase the energy resolution in the spectrum by effectively doubling the propagation time.[35] To avoid nonphysical reflections or wraparounds of the WP at the grid boundaries, it is multiplied by a damping function[36] at each time step activated at $R = 10.64a_0$ and $r = 5.307a_0$. Sufficiently large widths of the absorbing regions were required to prevent the reflection of the very low translational energy component of the WP, which arises from the dissociative states of ClH_2. We performed several test calculations and optimally chosen the widths of the absorbing regions as noted already. For example, increasing the width of the absorbing region by an approximate factor of 2 in either direction does not alter the final results.

We first carried out uncoupled surface (both diabatic and adiabatic) calculations. The peaks observed in the uncoupled $^2\Sigma_{1/2}$ adiabatic spectrum were then analyzed by fitting each of them to a Lorentzian line-shape function

$$Y(E) = Y_0 + \frac{2A}{\pi}\frac{w}{4(E - E_0)^2 + w^2} \tag{9}$$

This enables us to accurately estimate the energy eigenvalue corresponding to the peak maximum. The peaks are generally contaminated with the neighboring states, and an estimate of the line width often becomes cumbersome and difficult. Whenever a peak is fitted reasonably well, the line width lifetime τ_n is calculated from the full width at half-maximum (fwhm) w of the Lorentzian function by $\tau_n = \hbar/w$.

Once the eigenvalue of a peak is determined, the corresponding eigenfunction is then calculated by the spectral quantization algorithm: by projecting a time-evolved WP onto the desired eigenstate (n) with eigenvalue E_n

$$\Psi_n(E) = \int_0^T e^{iE_n t/\hbar}\Psi(t)\, dt \tag{10}$$

Subsequently, we carried out coupled-states calculations by considering the electronic and also the electronic-plus-SO couplings separately and investigated their role on the overall vibronic structure of each SO state. Finally, the role of the surface coupling on the different eigenstates of the $^2\Sigma_{1/2}$ adiabatic states is examined, and the time-dependent dynamics is discussed.

III. Results and Discussion

In this section, we present and discuss the results obtained by the formalism described in the preceding section. We first discuss the uncoupled-state spectra and analyze the peaks obtained therein. The implication of the surface coupling effects is considered thereafter. Finally, we show the photodetachment spectrum of ClD_2^- and compare the results with experimental observations.

A. Uncoupled Adiabatic and Diabatic Surface Results. To carry out a detailed investigation of the resonances in Cl(^{2}P) + H_2 system, we first report the energy-level spectrum of the uncoupled $^2\Sigma_{1/2}$, $^2\Pi_{3/2}$, and $^2\Pi_{1/2}$ adiabatic and diabatic CW PESs. We note that the primary aim of this article is to examine the surface coupling effects on the eigenstates of the $^2\Sigma_{1/2}$ adiabatic state which are important for the Cl(^{2}P) + H_2 reaction dynamics. The eigenstates of the component Π states are only considered briefly. The calculations are carried out by locating the initial GWP in the van der Waals region of these surfaces as well as in the barrier (TS) region of the $^2\Sigma_{1/2}$ PES. The initial locations and the width parameters of the GWPs used in various calculations reported here are given in Table 1. We note that locating the initial WP at $\gamma^\circ = \pi/2$ for a particular value of R° and r° yields an identical energy spectrum as for $\gamma^\circ = 0$ or π. The relative intensity of the peaks only differ in the two. In view of the fact that the photodetachment of ClH_2^- samples the collinear configurations of the ClH_2 PESs initially, we show the results here obtained by locating the initial wave packet at $\gamma = 0$ or π.

TABLE 1: Parameters for the Different Choices of the Initial Gaussian Wave Packet Used in Time Evolution

GWP	R_0 (a_0)	r_0 (a_0)	γ_0 (rad)	δ_R (a_0)	δ_r (a_0)	δ_γ (rad)	$\langle E\rangle$ (eV)
1	5.58	1.402	0.0	0.28	0.24	0.2	0.4868
2	6.04	1.402	0.0	0.25	0.25	0.2	0.4827
3	6.11	1.402	0.0	0.28	0.24	0.2	0.4698
4	6.26	1.402	0.0	0.25	0.24	0.2	0.4733
5	6.56	1.402	0.0	0.25	0.24	0.2	0.4697
6	3.658	1.814	0.0	0.3	0.4	0.2	0.6164
7	4.475	2.049	0.0	0.4	0.3	0.2	1.0381
8	4.599	2.136	0.0	0.3	0.4	0.2	1.2106
9	4.475	2.409	0.0	0.3	0.4	0.2	1.3137
10	4.843	2.387	0.0	0.3	0.4	0.2	1.6763

The pseudospectra obtained by initially locating the GWP nos. 2 and 7 on the $^2\Sigma_{1/2}$ adiabat are shown in Figure 2a and b, respectively. The spectra are obtained through eq 1, and the decay of the corresponding autocorrelation functions is included as inserts in the respective figures. The peaks in Figure 2a correspond to the progression of low-energy van der Waals resonances arising from the shallow well region of the Cl + H_2 asymptote, whereas those in the Figure 2b correspond to the high-energy resonances arising from the barrier region of the PES. The location of the initial WP on the PES corresponds to an average energy $\langle E\rangle = 1.038$ eV for the spectrum in Figure 2b. This leads to the resolved structure of the high-energy peaks in the spectrum. The low-energy peaks are also obtained with this WP but are much less resolved than in Figure 2a. The analysis of the individual peaks of Figure 2a,b is discussed in the text to follow.

The pseudospectra obtained with the GWP nos. 2 and 7 on the $^2\Sigma_{1/2}$ diabat are shown in Figure 3a,b. The decay of the corresponding autocorrelation function is also included as an insert in the respective panel. It can be seen from Figure 3a that the low-energy diabatic spectrum is less structured than the corresponding adiabatic spectrum shown in Figure 2a. The high-energy spectrum in Figure 3b more closely resembles that in Figure 2b. However, the high-energy diabatic spectrum in Figure 3b is relatively more structural than the corresponding adiabatic spectrum in Figure 2b. The differences between the adiabatic and diabatic results may be due to the fact that a diabatic state represents an admixture of the adiabatic states. The extent of mixing depends on the nuclear coordinates, which is different for the location of the initial WP in the van der Waals well and the barrier regions of the PES. We note that, although we calculate the diabatic $^2\Sigma_{1/2}$ spectra for comparison, we will concentrate on the more realistic adiabatic $^2\Sigma_{1/2}$ spectra (cf. Figure 2a,b) in the rest of our discussions.

We also calculated the adiabatic and diabatic $^2\Pi_{3/2}$ and $^2\Pi_{1/2}$ spectra. These two surfaces are closed along the channel leading to the ground-state products. Therefore, the vibrational structure

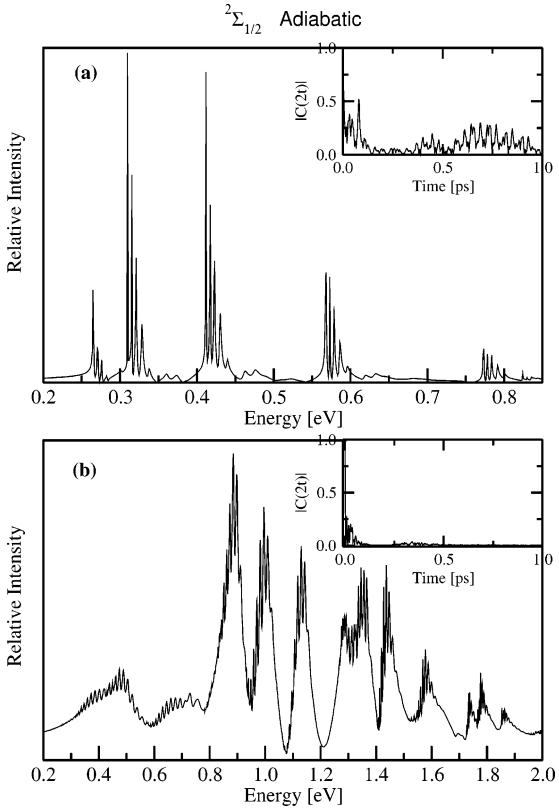

Figure 2. The pseudospectrum of the quasi-bound states of the uncoupled $^2\Sigma_{1/2}$ adiabatic electronic state of ClH_2. The two spectra in panels (a) and (b) are obtained with GWP nos. 2 and 7, respectively. The intensity in arbitrary units is plotted as a function of the energy of the $^2\Sigma_{1/2}$ electronic state. The energy corresponding to peak maxima represents the eigenvalue of the quasi-bound state. The zero point of energy corresponds to the asymptotically separated Cl + H_2 species on the $^2\Sigma_{1/2}$ electronic state. The decay of the absolute value of the corresponding autocorrelation function $|C(2t)|$ in time is shown as an insert in the respective panels.

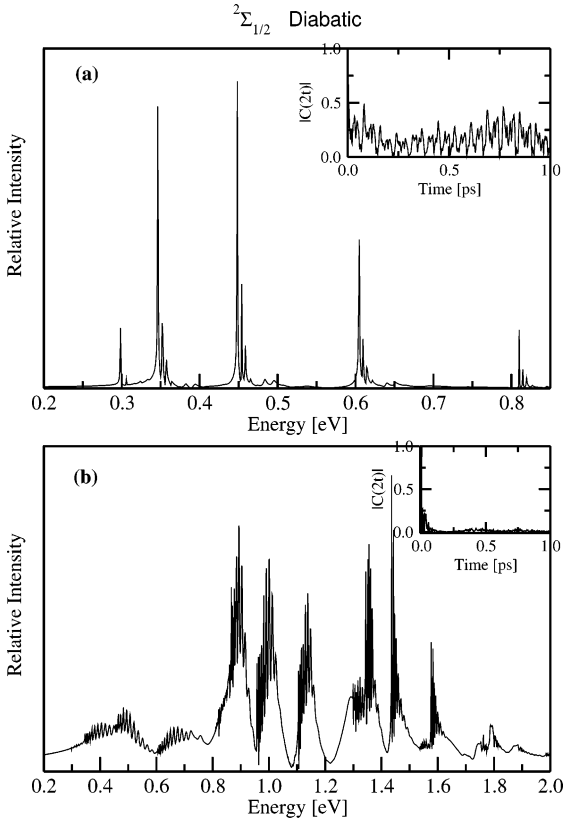

Figure 3. Same as in Figure 2, for the uncoupled $^2\Sigma_{1/2}$ diabatic electronic state.

of the spectrum obtained on these surfaces reveals the spectroscopy of the reagent van der Waals well region only. The resulting spectra show analogous vibrational structure as seen in the low-energy $^2\Sigma_{1/2}$ spectra in Figure 2a and Figure 3a, and we do not show them here. We note that the adiabatic results for the component $^2\Pi$ state has been shown in our previous article on the photodetachment spectrum of ClH_2^-.[12] As seen previously, the spectra reveal a progression of envelopes, and the fine structures under each envelope correspond to the progression along the Cl···H_2 dissociation coordinate. An energy shift of ~0.1 eV of the 0−0 peak corresponding to the SO splitting of the component Π states has been observed in the two spectra. The spectra for the component $^2\Pi$ state do not reveal any structure at high energy. As mentioned already, these two states are closed along the *r* coordinate. This also explains the strong similarity observed for the $^2\Sigma_{1/2}$ adiabatic (cf. Figure 2b) and diabatic (cf. Figure 3b) results at high energies.

B. Resonances of the Uncoupled $^2\Sigma_{1/2}$ Adiabatic State. The quasi-bound spectrum of the $^2\Sigma_{1/2}$ adiabatic electronic state is the most crucial governing factor of the outcome of the Cl(^{2}P) + H_2 reaction. Because the adiabatic electronic representation gives a realistic description of the observables in an experiment, in this section we make an effort to analyze the peaks observed in the adiabatic $^2\Sigma_{1/2}$ spectra shown in Figure 2a,b. We mention that, apart from the two spectra shown in Figure 2a,b, we have computed a number of additional spectra by varying the initial location of the GWP (as described in Table 1) in order to check the commonality of peaks observed in different spectra. The peak energies and widths are computed by fitting them to a Lorentzian line shape function, and their eigenvectors are computed by the spectral quantization algorithm as described in section II. The minimum of the van der Waals well on the $^2\Sigma_{1/2}$ adiabatic state occurs at a C_{2v} configuration of ClH_2 at $R \approx 5.78a_0$. The low-energy spectrum shown in Figure 2a corresponds to the vibrational structure of the prereactive van der Waals complex. The barrier on the $^2\Sigma_{1/2}$ adiabatic state, on the other hand, occurs at the collinear configuration of ClH_2 and a shorter value of $R \approx 3.631a_0$.[10] Therefore, the peaks observed in the spectrum in Figure 2b are expected to reveal the spectroscopy of the TS region of the $^2\Sigma_{1/2}$ electronic state.

The energy eigenvalue and lifetime of the resonances extracted from various spectra (calculated in the present study) are collected in Table 2. We note that a blank entry in Table 2 represents an uncertainty in estimating the corresponding peak width. Lorentzian line shape fittings of two typical peaks are shown in Figure 4a,b. The asterisks in the figure represent the computed points, while the solid curves represent the best-fit Lorentzian. The fitting in Figure 4a represents a difficult situation where the energy eigenvalue corresponding to the peak maximum can be extracted; however, the peak width cannot be reliably estimated. The fitting shown in Figure 4b, on the other hand, represents the situation where both the parameters can be reliably estimated.

The eigenfunctions of a few representative resonances of the uncoupled $^2\Sigma_{1/2}$ adiabatic state are shown in Figures 5a−n and 6a−h. While the eigenfunctions in Figure 5a−n represent the low-energy van der Waals resonances, those in Figure 6a−h represent the high-energy resonances arising from the TS region of the PES. Eigenfunctions are plotted in terms of the probability density ($|\Psi|^2$) contours in the (R, r) and (γ, R) planes averaged over γ and r, respectively, to clearly identify their nodal patterns

TABLE 2: Eigenvalues (E_n's), Assignments, and the Line Width Lifetime of the Quasi-Bound States of ClH_2 on the $^2\Sigma_{1/2}$ Adiabatic Electronic State[a]

eigenvalue (eV)	assignment (n_R,n_r,n_γ)	lifetime (fs)	eigenvalue (eV)	assignment (n_R,n_r,n_γ)	lifetime (fs)
0.264	(0,0,0)		0.885	(7,1,2)	87
0.271	(1,0,0)		0.899	(8,1,2)	62
0.275	(2,0,0)		0.912	(9,1,2)	44
0.283	(3,0,0)	38	9.22	(0,1,4)	
0.310	(0,0,2)		0.928	(1,1,4)	
0.315	(1,0,2)	173	0.932	(2,1,4)	
0.320	(2,0,2)	145	0.940	(3,1,4)	
0.327	(3,0,2)	221	0.948	(4,1,4)	121
0.339	(4,0,2)	93	0.959	(5,1,4)	186
0.347	(5,0,2)		0.970	(6,1,4)	126
0.362	(6,0,2)	117	0.983	(7,1,4)	111
0.375	(7,0,2)	102	0.997	(8,1,4)	73
0.387	(8,0,2)	82	1.011	(9,1,4)	67
0.404	(9,0,2)	60	1.022	(0,0,10)	
0.411	(0,0,4)	500	1.026	(1,0,10)	
0.417	(1,0,4)	308	1.032	(2,0,10)	
0.423	(2,0,4)		1.040	(3,0,10)	
0.431	(3,0,4)	245	1.051	(4,0,10)	150
0.441	(4,0,4)	80	1.070	(0,1,6)	
0.450	(5,0,4)	158	1.080	(2,1,6)	
0.465	(6,0,4)		1.088	(3,1,6)	
0.478	(7,0,4)	194	1.097	(4,1,6)	
0.490	(8,0,4)	91	1.107	(5,1,6)	197
0.506	(9,0,4)	91	1.118	(6,1,6)	118
0.522	(10,0,4)	54	1.131	(7,1,6)	99
0.568	(0,0,6)	232	1.144	(8,1,6)	
0.573	(1,0,6)		1.156	(9,1,6)	45
0.579	(2,0,6)	267	1.264	(0,1,8)	
0.587	(3,0,6)	160	1.270	(1,1,8)	
0.596	(4,0,6)		1.276	(2,1,8)	
0.605	(5,0,6)	307	1.282	(3,1,8)	
0.621	(6,0,6)	121	1.293	(4,1,8)	
0.635	(7,0,6)	132	1.131	(5,1,8)	103
0.668	(8,0,6)	45	1.325	(6,1,8)	27
0.684	(9,0,6)	68	1.336	(7,1,8)	233
0.773	(0,0,8)		1.346	(8,1,8)	169
0.778	(1,0,8)		1.356	(9,1,8)	91
0.784	(2,0,8)		1.401	(0,2,4)	
0.792	(3,0,8)		1.408	(1,2,4)	
0.824	(0,1,2)		1.414	(2,2,4)	
0.829	(1,1,2)	158	1.425	(3,2,4)	
0.835	(2,1,2)		1.427	(4,2,4)	228
0.844	(3,1,2)	132	1.437	(5,2,4)	119
0.851	(4,1,2)	115	1.448	(6,2,4)	68
0.862	(5,1,2)	197	1.460	(7,2,4)	53
0.873	(6,1,2)		1.473	(8,2,4)	22

[a] A blank entry indicates the corresponding quantity could not be determined unambiguously.

revealing the progression of the resonances. Each feature of the eigenvalue spectra (cf. Figure 2a,b) can be associated with a stationary wave function. All of the eigenstates documented in Table 2 are assigned by inspecting their nodal patterns along R, r, and γ. They are identified in terms of three quantum numbers n_R, n_r, and n_γ representing the number of nodes along these coordinates, respectively. We note that we show plots of only a few eigenstates here, to discuss the details. The eigenfunction in Figure 5a has no node along R, r, or γ and therefore represents the (0, 0, 0) state according to the (n_R, n_r, n_γ) assignment. It is interesting to see that the probability maximum of this function occurs at a stretched configuration of ClH_2 along R ($6.0a_0 \leq R \leq 7.5a_0$), indicative of the van der Waals nature of the interaction along this coordinate. A heavy buildup of the probability density at $\gamma = \pi/2$ can be seen from the (γ, R) plot. This indicates that the van der Waals minimum occurs at the bent configuration of ClH_2. Furthermore, the wave function is highly diffuse along γ. The eigenfunction in Figure 5b has one node along R and no nodes along r and γ. It is a (1, 0, 0) state. The next eigenfunction (Figure 5c) has two nodes along γ and is a (0, 0, 2) state. We note that even quantum progression is only observed along the angle γ. The latter represents the bending motion of the ClH_2 complex. For each value of n_γ, we find an envelope with fine structures in Figure 2. The fine structures within each envelope reveal progression along the R coordinate. This is illustrated by the eigenfunctions in Figure 5d,e. For each of these two functions, $n_\gamma = 2$, whereas $n_R = 2$ for the former and $n_R = 7$ for the latter. The next three eigenstates in Figure 5f−h have four quantum excitations along γ (i.e., $n_\gamma = 4$). The next four eigenstates (cf. Figure 5i−l) correspond to $n_\gamma = 6$. The eigenstate in Figure 5i is a (1, 0, 6) state, and those in Figure 5j, 5k, and 5l are (3, 0, 6), (7, 0, 6), and (9, 0, 6) states, respectively. The eigenstates in Figure 5m and 5n have eight quantum excitations along γ and represent the (0, 0, 8) and (3, 0, 8) states, respectively.

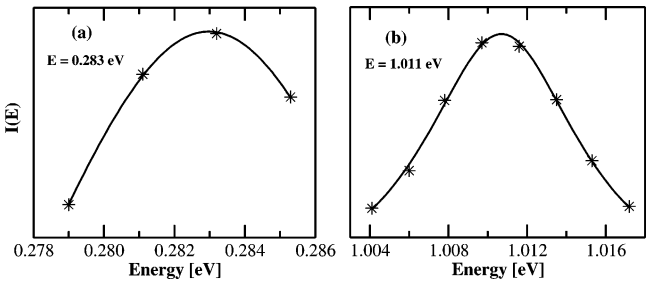

Figure 4. Lorentzian line shapes for the two typical spectral peaks centered at $E = 0.283$ eV and $E = 1.011$ eV, shown by the solid curve in panels (a) and (b), respectively. The results obtained from the time-dependent WP calculations are shown by the asterisks. While the peak in panel (a) represents the case where the energy eigenvalue can be estimated accurately but width cannot be, the one in panel (b) represents the case where both of these quantities can be determined with reasonable accuracy.

It can be seen that none of the eigenstates mentioned in the preceding paragraph reveal a progression along the r coordinate. The latter represents the vibrational motion of the H_2 moiety. In Figure 6a−h, we show some representative eigenfunctions obtained from the peaks observed at the high-energy part of Figure 2a,b. The eigenstate in Figure 6a reveals one quantum excitation along H_2 vibrational coordinate and may be assigned as a (0, 1, 4) state. When compared with the (0, 0, 4) state in Figure 5f, one can see that this state is ~0.5 eV higher in energy corresponding to the $\upsilon = 0 \rightarrow \upsilon = 1$ vibrational excitation of H_2. The eigenstates in Figure 6b,c occur under the same envelope with the one in Figure 6a. They all have $n_\gamma = 4$ and reveal a progression along the R motion. The other eigenstates in Figure 6d,e,f,g,h represent (0, 0, 10), (0, 1, 6), (4, 1, 6), (3, 2, 6), and (4, 2, 6) states, respectively, according to the (n_R, n_r, n_γ) assignment. We note that the overall structures of most of the eigenstates described in Figures 5 and 6 reveal the feature of a continuum wave function when viewed along R and γ coordinates.

C. Coupled-States Results: Electronic and Spin−Orbit Coupling. In this section, we will discuss the effects of the electronic and SO coupling on the spectra discussed already. For the low-energy part of the spectra, these effects have been discussed in a previous publication dealing with the photodetachment of ClH_2^-.[12] Therefore, we concentrate here on the high-energy part of the spectra. We note that a diabatic electronic representation is utilized throughout in calculating the coupled-states spectra. This is primarily to restore uniformity, because for the 3×3 coupled-states problem, an acceptable definition of the adiabatic-to-diabatic transformation matrix is still a

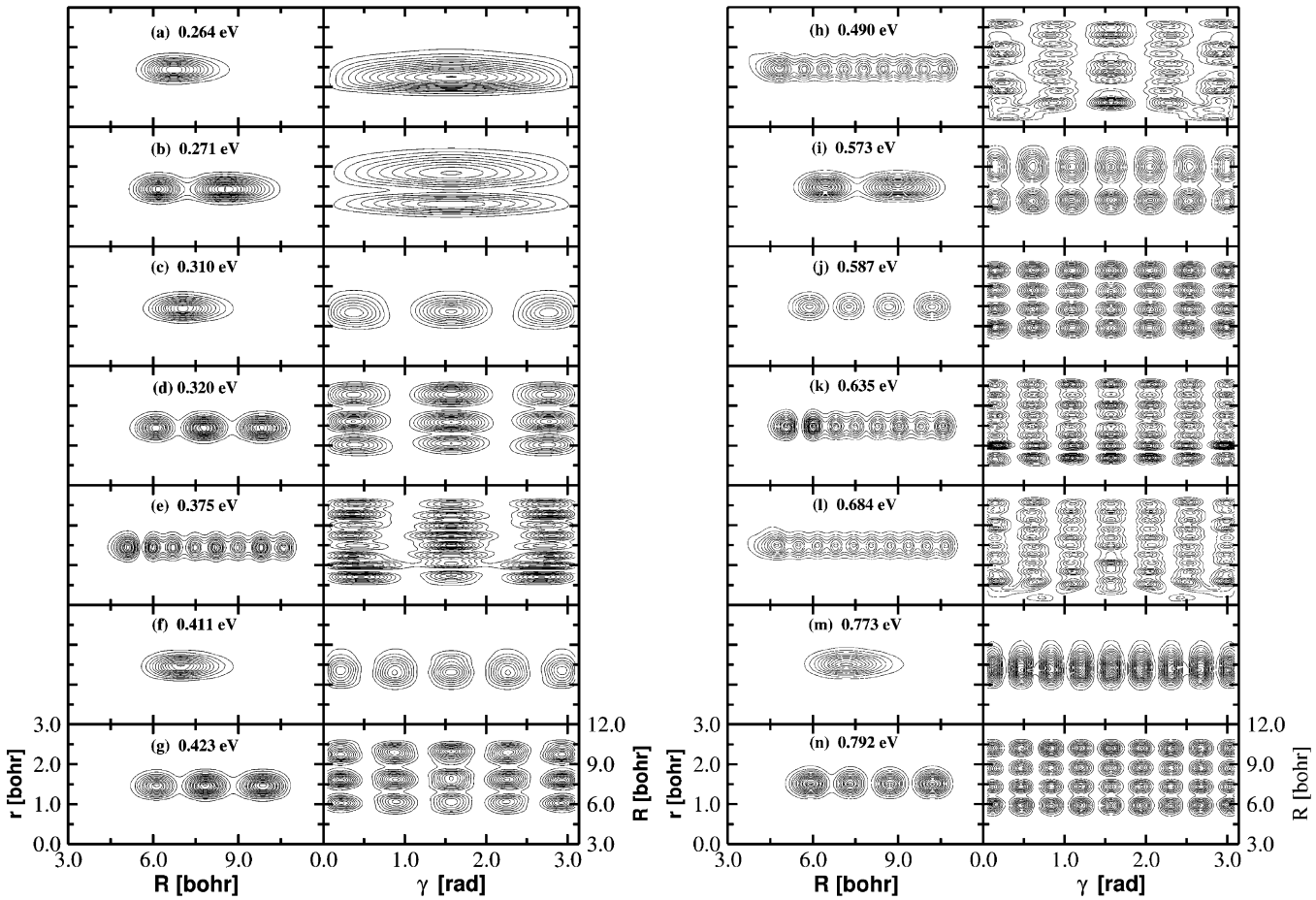

Figure 5. Probability density contours of the quasi-bound eigenfunctions obtained through the spectral quantization algorithm (eq 10). The energy eigenvalues of the quasi-bound states are indicated in the respective panel, and the contour plots are shown in both the (R, r) and (γ, R) planes for average values of γ and r, respectively.

complicated issue. Therefore, the uncoupled diabatic spectra shown already are to be considered when comparing with the coupled-state results presented in the following text.

The coupled $^2\Sigma_{1/2}$ diabatic spectra are presented in Figure 7a,b. These spectra are obtained with GWP no. 7, and the corresponding uncoupled $^2\Sigma_{1/2}$ diabatic spectrum is shown in Figure 3b. The spectra in Figure 7a and b are obtained by considering the electronic (only) and electronic-plus-SO coupling, respectively. As can be seen by comparing with the uncoupled-state spectrum of Figure 3b, the electronic coupling does not have any noticeable impact on the spectrum (cf. Figure 7a). On the other hand, the spectrum becomes more diffuse and structureless with the inclusion of the SO coupling in the dynamics. This reveals that the nonadiabatic effects due to SO coupling are stronger in the $Cl(^2P) + H_2$ dynamics. This leads to a considerable mixing of the interacting electronic states and an increase of the line density in the spectrum. Because of the appearance of numerous closely spaced lines, the spectral envelope appears to be more diffuse and structureless. The effect of the electronic and SO coupling on the low-energy part of the component's $^2\Pi$-state spectra has been discussed before.[12] Because the high-energy spectra of these states are structureless, we will no longer consider them here.

D. Time-Dependent Dynamics of the Quasi-Bound States of the $^2\Sigma_{1/2}$ Adiabatic State. To investigate the effects of electronic and SO coupling on the quasi-bound states of the $^2\Sigma_{1/2}$ adiabat more closely, we examine their time evolutions in the uncoupled- and coupled-state situations. In Figure 8a−h, we show the eigenvalue spectrum and the survival probability ($|C(t)|^2$) of four quasi-bound states corresponding to resonances indicated in the respective panels. The survival probability of the resonance in panel a is shown in panel b, that of panel c is shown in panel d, and so on. In each panel, the solid line indicates the result obtained in the uncoupled-state situation, and those obtained with the electronic and electronic-plus-SO coupling in the coupled-state situation are shown by the dashed and dotted lines, respectively. The eigenvalue spectra in Figure 8a correspond to the resonances shown in Figure 5a. It can be seen that the peak maxima (referring to the energy eigenvalues of the resonance) shift to higher energy by ∼0.032 eV when electronic coupling is considered in the dynamics. This kind of shift of energy eigenvalue in the coupled-state dynamical study has been reported previously in the literature and is attributed to the geometric phase change of the adiabatic electronic wave function while encircling the conical intersection in a closed loop.[31,37] The spectral peak splits into two (dotted line) when both the electronic and SO coupling are included in the dynamics. The two peaks are separated by ∼0.112 eV in energy, which is nearly equal to the magnitude of the SO splitting of the interacting states (cf. Figure 1).

The survival probability plot of the mentioned resonance shown in panel b reveals interesting dynamical features. The initial decay of the resonance is very very slow (cf. solid line) in the uncoupled-state situation, which indicates a long lifetime of this quasi-bound state and therefore reveals a bound-state character of this state. The inclusion of the electronic coupling leads to a relatively faster decay (cf. dashed line) of the same, due to a nonadiabatic transition to the $^2\Pi$ electronic state. A

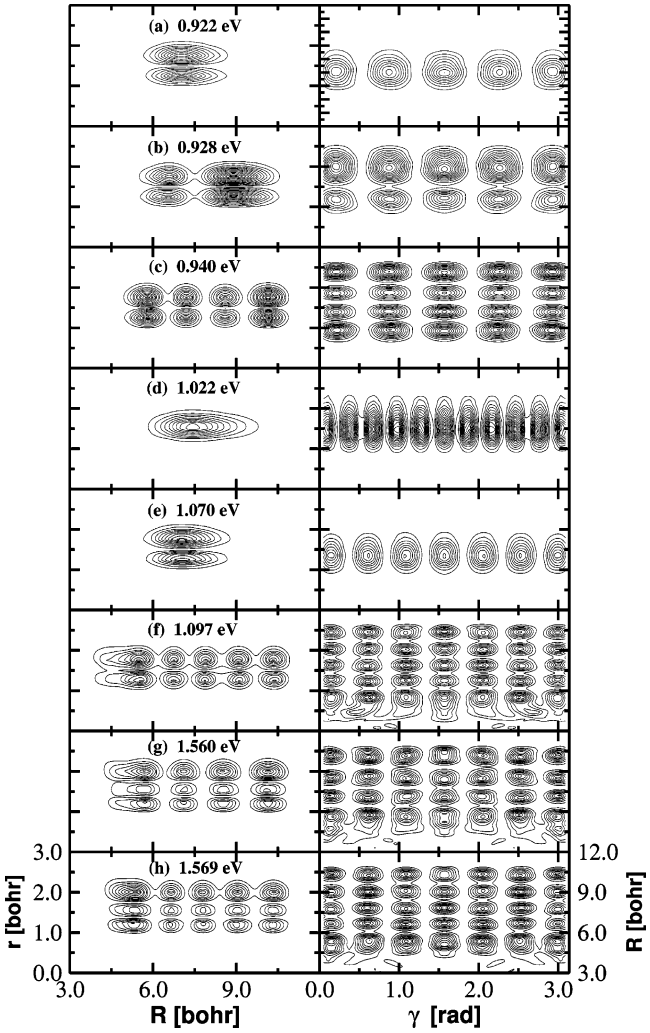

Figure 6. Same as in Figure 5.

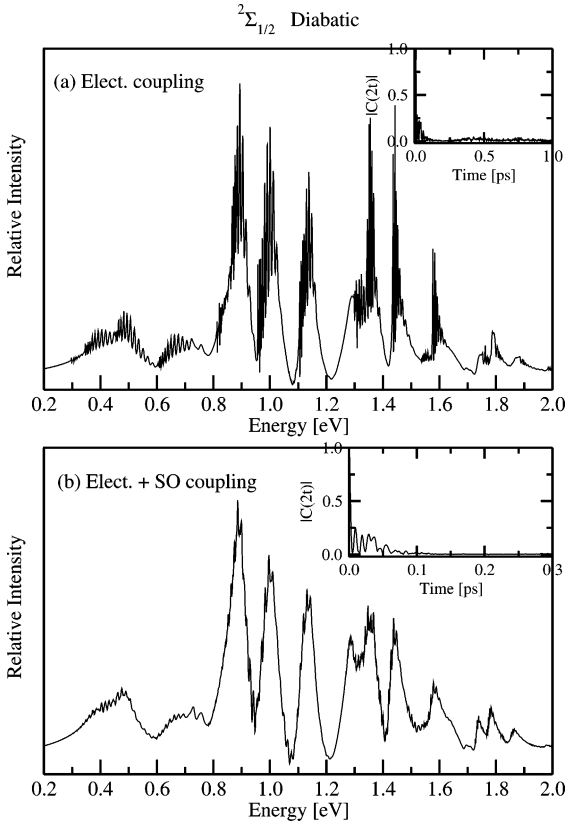

Figure 7. Quasi-bound spectrum of the $^2\Sigma_{1/2}$ diabatic electronic state in the coupled-state situation obtained with GWP no. 7. The spectrum in panel (a) is calculated by considering the $\Sigma-\Pi$ electronic coupling only. The spectrum in panel (b), on the other hand, is calculated by considering both the electronic and SO coupling. The decay of the absolute value of the corresponding $C(2t)$ is shown as an insert in the respective panels.

nonradiative transition time of ~250 fs can be discerned from the plot. In addition to the electronic coupling, when the SO coupling is included in the dynamics, nonadiabatic transitions to the component ($^2\Pi_{3/2}$ and $^2\Pi_{1/2}$) states are possible, and as a result, one finds a rapid oscillatory pattern in the corresponding survival probability curve (cf. dotted line). The recurrences are ~36-fs spaced in time. The latter corresponds to the ~0.112-eV spacing of the observed peaks in Figure 8a (cf. dotted line).

Analogous features of the eigenvalue spectra and the survival probabilities are obtained for the (1, 0, 2) and (1, 0, 6) resonances shown in Figure 8c,d and e,f, respectively. Generally, the bending excitation leads to somewhat slower decay of the resonances, which becomes more rapid when ClH_2 is excited along the *R* coordinate. The results shown in Figure 8g,h correspond to the (4, 2, 6) eigenstate shown in Figure 6h. In this case, the state reveals much faster decay. The initial fast decay of the survival probability relates to a decay time of ~230 fs in the uncoupled-state situation. This decay time is further reduced in the coupled-state situation. A decay time of ~70 fs can be estimated from the survival probability curves with electronic and electronic-plus-SO coupling. An energy shift of ~0.035 eV in the eigenvalue of the resonances estimated with electronic coupling remains almost the same in all the spectra shown in Figure 8. Also, the splitting in energy of ~0.110 eV of the doublet peak structure when both the electronic and electronic-plus-SO coupling are considered nearly remains the same.

To this end, it is worthwhile to briefly discuss the electronic population dynamics in the coupled-state situations mentioned in the preceding paragraph. It is probably not relevant to discuss this for each of the quasi-bound states shown already, and we typically select the quasi-bound state of Figure 6g for the following discussion. In Figure 9a,b, we show the time dependence of the adiabatic and diabatic electronic populations. While the populations shown in Figure 9a consider the electronic coupling alone, both the electronic and SO couplings are considered in Figure 9b. Because in the latter case, the whole investigation is carried out in a diabatic electronic representation, we show the diabatic electronic populations only.

In Figure 9a, the adiabatic and the diabatic electronic populations are indicated by the solid and dashed lines, respectively. The initial WP (the (4, 2, 6) eigenstate) is located on the $^2\Sigma$ diabat, and therefore, the population of this state is 1.0 (upper dashed curve), and that of the $^2\Pi$ state (lower dashed curve) is 0.0 at $t = 0$. The population of the $^2\Sigma$ diabat decreases slightly, and that of the $^2\Pi$ diabat grows to the same extent in time. It is evident from the figure that, even for this high-energy quasi-bound state, only a small fraction of the WP transits to the $^2\Pi$ surface. Because this transition is solely caused by the $\Sigma-\Pi$ electronic coupling, the latter seems to be very weak and does not have much impact on the dynamics. This is also revealed in the energy spectrum discussed in Figure 7a. The initial location of the WP for the population curves in Figure 9a corresponds to an admixture of the $^2\Sigma-^2\Pi$ adiabatic states. Therefore, a 65% (35%) population of the $^2\Sigma$ ($^2\Pi$) adiabatic states is obtained at $t = 0$. Afterwords, the population exchange between the two surfaces through the $\Sigma-\Pi$ conical intersection is clearly revealed by the figure.

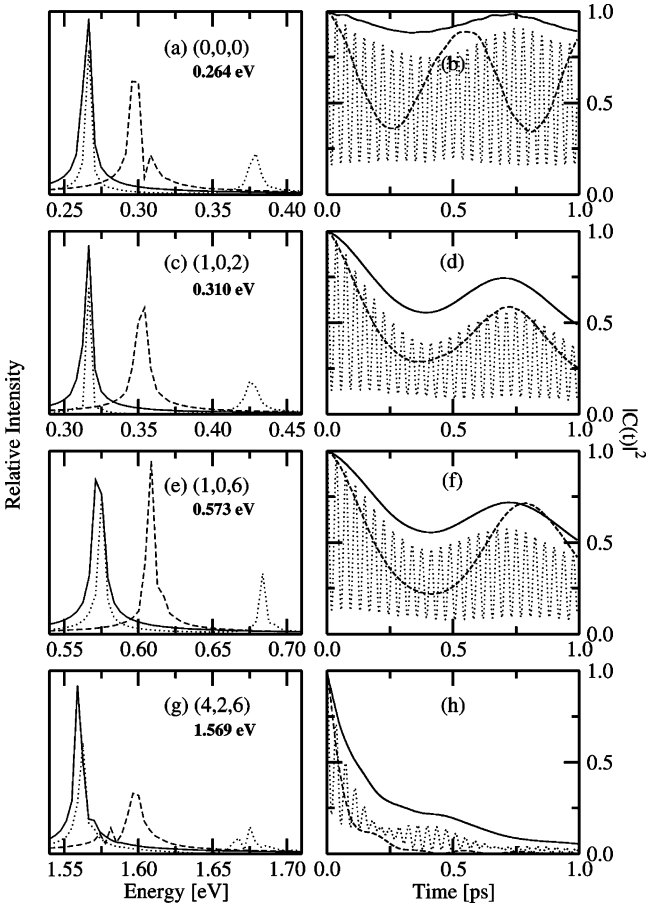

Figure 8. Impact of the electronic and electronic-plus-SO coupling on the quasi-bound spectrum of the individual eigenstates (indicated in the panel) of the $^2\Sigma_{1/2}$ adiabatic electronic state. The spectra obtained in the uncoupled (solid line) and coupled [electronic only (dashed line) and electronic-plus-SO (dotted line)] state situations are shown in the panels in the left column of the figure. The time dependence of the corresponding survival probabilities are plotted in the adjacent panels in the right column of the figure.

The time dependence of electronic populations of the $^2\Sigma_{1/2}$ and two components of the $^2\Pi$ diabatic states in the presence of the electronic and SO coupling are shown in Figure 9b. The electronic population of the $^2\Sigma_{1/2}$ diabatic state is shown by the solid line, whereas that of the components of the $^2\Pi$ diabatic states are shown by dotted and dashed lines, respectively. In this case, because the SO coupling is also activated in addition to the $\Sigma-\Pi$ electronic coupling, a considerable population exchange with the component $^2\Pi$ states is also seen. Because the WP is initially located on the $^2\Sigma_{1/2}$ diabat, the population of this state is 1.0 at $t = 0$. It can be seen that the populations of the $^2\Sigma_{1/2}$ and one of the components (with energy of $V_\Pi + A$) of the $^2\Pi$ diabat fluctuate uniformly in time, indicating the exchange of populations between these states mediated mostly by the SO interactions. The recurrences in the population curves are ~36-fs spaced in time, which amounts to an energy spacing of ~0.112 eV, nearly corresponding to the SO coupling strength of atomic Cl. The growth in population of the second component (with energy of $V_\Pi - A$) of the $^2\Pi$ diabat in time is very small, indicating that the nuclear dynamics on the $^2\Sigma_{1/2}$ diabatic state is not very much affected by this state.

E. Photodetachment Spectrum of ClD_2^- and Comparison with Experiment. Photodetachment spectroscopy of ClH_2^- and ClD_2^- is of considerable interest, because it is found to successfully probe the prereactive van der Waals well in the bimolecular $Cl(^2P) + H_2$ (D_2) reaction. The photodetachment

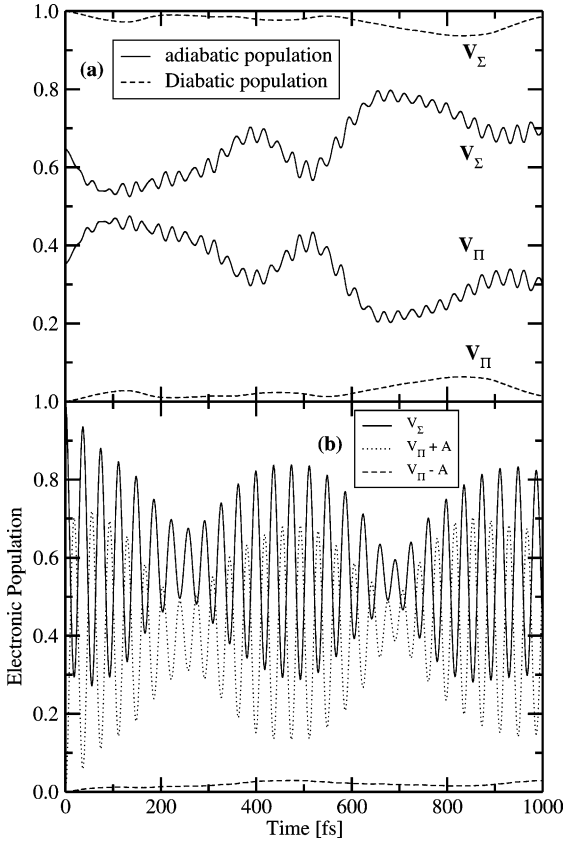

Figure 9. Time dependence of the electronic population in the coupled-state dynamics of the eigenstate of Figure 8g. The adiabatic (solid line) and diabatic (dashed line) electronic populations in panel (a) are obtained with the $\Sigma-\Pi$ electronic coupling only. The diabatic electronic populations of the three SO states when both the electronic and SO coupling are included in the dynamical simulation are shown in panel (b).

spectrum of ClD_2^- is examined here by using the same strategy employed in our earlier work on ClH_2^-.[12] The photodetachment spectra of these two isotopomers differ considerably in terms of the widths of the observed peaks.[16] The peaks in the ClD_2^- spectrum are much broader than those in the ClH_2^- spectrum.[16] The possible excitation of the hinder rotor levels in the ClD_2^- transition has recently been pointed out by Osterwalder et al.[17] The nuclear wave function for the ground electronic state of ClD_2^- is approximated with the stationary GWP of eq 8. This wave function is initially located at the near-equilibrium geometry of ClD_2^- at $R^0 = 5.97a_0$, $r^0 = 1.402a_0$, and $\gamma^0 = 3.14$ rad and subjected to an FC transition to the coupled electronic states of neutral ClD_2. The WP on this final electronic manifold is propagated in time with the aid of the coupled-state Hamiltonian of eq 6 for $\mathbf{J} = 0.5$. The photodetachment spectrum is calculated by Fourier transforming the time autocorrelation function of the WP to the energy domain.

The calculated photodetachment spectrum of ClD_2^- along with the experimental results of Neumark and co-workers[16] are shown in Figure 10. The relative intensity in arbitrary units is plotted as a function of the energy of the final electronic manifold in electronvolts. The theoretical spectrum is obtained in the following way: The spectra pertinent to a transition to each of the $^2\Sigma_{1/2}$, $^2\Pi_{3/2}$, and $^2\Pi_{1/2}$ diabatic electronic states in the coupled-state situation are calculated. The resulting three partial spectra are then combined and convoluted with a Lorentzian function of 24 meV fwhm to calculate the spectral envelope shown in Figure 10. The relative height of the two peaks is adjusted in order to better match the theoretical data

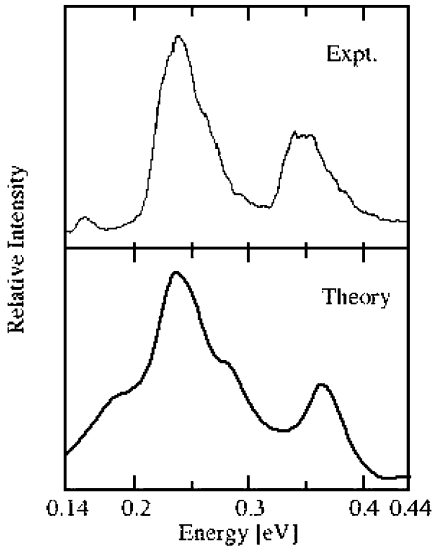

Figure 10. The photodetachment spectrum of ClD_2^-. The 299-nm experimental results are reproduced from ref 16 and shown in the top panel. The time-dependent WP results at low resolution are shown in the bottom panel. The relative intensity is plotted in arbitrary units as a function of energy of the final electronic state. The zero of energy corresponds to the asymptotically separated Cl + D_2 fragments on the $^2\Sigma_{1/2}$ adiabatic state.

with the experimental results. This is because equal values of the transition dipole matrix elements were assumed in the calculation of the three partial spectra; therefore, such an adjustment was necessary.

The convergence of the three partial spectra is checked by varying the length of the time propagation and also the width of the absorbing region along *R* and *r*. The spectrum shown in Figure 10 is obtained by propagating the WP for a total of ~1.8 ps with a time step of ~0.109 fs. The width of the absorbing potential is set to $7.84a_0$ and $3.92a_0$ along *R* and *r*, respectively. It can be seen from Figure 10 that the theoretical result is in good accord with the experimental observation. In the experimental results, the two peak maxima were estimated at 3.697 and 3.806 eV, and their separation of 0.109 eV corresponds to the Cl SO splitting. Despite a good overall agreement between the theoretical and experimental results, the separation between the peak maxima is ~0.03 eV higher in the theoretical results. It is to be noted that the theoretical result is obtained by propagating WP, and it is known that the spectrum generated by this method is usually associated with background contributions arising from the direct dissociative component of the WP. Our foregoing discussions reveal that this problem is even more severe in the present case, as the majority of the quasi-bound states have the feature of a continuum state. Therefore, a part of the difference between the theoretical and experimental results in Figure 10 can be attributed to this. A second source for the difference can be attributed to the approximate adjustment of the transition dipole matrix elements, which are assumed to be constants, and to the accuracy of the neutral electronic PESs and their coupling surfaces as well as the initial wave function of ClD_2^-, which has been approximated to a stationary GWP in the present study.

In the experimental spectrum, the first broad peak is assigned to a transition to the SO ground state ($^2\Pi_{3/2}$) and the second small peak to the SO excited state ($^2\Pi_{1/2}$) of ClD_2. An examination of the theoretical results reveal that each peak originates from clusters of transitions, and the vibrational structure of each peak is quite complex. Much of the complexity arises from the nonadiabatic effects due to SO interactions of the participating electronic states of ClD_2. The major contribution to the first broad peak comes from the transition to the $^2\Pi_{3/2}$ state. Also, a substantial contribution comes from a transition to the $^2\Pi_{1/2}$ state to the second peak.

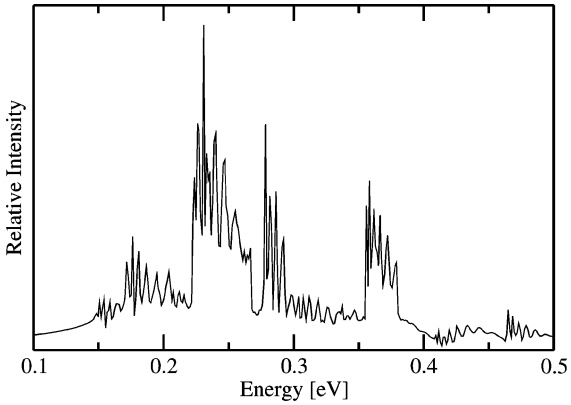

Figure 11. The time-dependent WP dynamical results, same as shown in Figure 10, at higher-energy resolution. The spectrum is obtained by adding three coupled-state spectra pertinent to the initial transition to each of the three SO states of ClD_2.

The theoretical WP result at higher-energy resolution is presented in Figure 11. This represents a combination of three partial spectra obtained from separate initial transitions to the $^2\Sigma_{1/2}$, $^2\Pi_{3/2}$, and $^2\Pi_{1/2}$ diabatic states of the neutral ClD_2. A convolution of this spectrum is shown in Figure 10. Quite similar peak structures have been reported by Manolopolous and Alexander in the FC simulation of the ClD_2^- spectrum.[20] Analogous to the ClH_2^- spectrum [cf. Figure 3a of ref 12], the ClD_2^- spectrum also reveals series of peaks which can be attributed to the progression along the *R* and γ coordinates. In the same energy range, transitions in ClD_2^- appear to be wider than in ClH_2^-, which contributes to the observed diffuse structure of the two peaks. The equilibrium geometry of ClD_2^- occurs at a somewhat shorter (by ~$0.1a_0$) distance than ClH_2^- along *R*. As a result, the WP in the case of the transition on ClD_2^- samples relatively more of the repulsive part of the SO states of ClD_2. The possible rotational excitations contributing to the peak structures are not examined here and will be addressed in a future publication.

IV. Summary

We presented a detailed theoretical account of the quasi-bound states corresponding to resonances in the Cl(^{2}P) + H_2 reaction dynamics of its ground $^2\Sigma$ electronic state. The quasi-bound states are obtained by examining a set of pseudospectra calculated with the aid of a time-dependent WP approach. These states are further characterized in terms of their eigenfunctions calculated by the spectral quantization algorithm. The impact of the electronic and SO coupling with the excited $^2\Pi$ electronic state on the resonances is examined in detail. Spectra are reported for both the uncoupled- and coupled-state situations. While both adiabatic and diabatic electronic representations are considered in the uncoupled-state situation, the diabatic electronic representation is considered only in the coupled-state situation. The low-energy quasi-bound spectra originating from the van der Waals well region of the uncoupled $^2\Sigma_{1/2}$, $^2\Pi_{3/2}$, and $^2\Pi_{1/2}$ electronic states revealed analogous features (viz., the progression of envelopes with fine structures underneath). The $^2\Pi_{3/2}$ and $^2\Pi_{1/2}$ electronic states are closed along the *r* coordinate leading to the ground-state products HCl($X^1\Sigma^+$) + H(^{2}S). The latter are produced only on the $^2\Sigma_{1/2}$ electronic state. Therefore, the high-energy quasi-bound spectrum of the $^2\Sigma_{1/2}$ electronic

state originating from the barrier region is also calculated and has revealed a similar progression of envelopes as stated already.

The quasi-bound spectrum of the $^2\Sigma_{1/2}$ adiabatic state is analyzed in detail. Each envelope in the spectrum corresponds to an even quantum excitation along the bending coordinate. The fine structures under each envelope correspond to an extended progression along the Cl···H_2 dissociation coordinate. The excitation of the H_2 vibration is observed only at high energies. The majority of the quasi-bound states revealed features of a continuum state.

The effect of the electronic coupling to the $^2\Pi$ state has only a minor impact on the overall structure of the quasi-bound spectrum of the $^2\Sigma$ state. However, the SO coupling has considerable effect on it. The line density in the spectrum increases significantly because of relatively strong nonadiabatic effects due to SO interactions, and the spectrum becomes more diffuse and structureless. Investigation of the impact of the electronic and SO couplings on the individual eigenstates of the $^2\Sigma_{1/2}$ adiabat revealed that the electronic coupling alone causes a shift in the energy of the peak maxima by ~0.035 eV. This is attributed to the geometric phase change of the adiabatic electronic wave function while encircling the $^2\Sigma-^2\Pi$ conical intersections in a closed loop. The electronic-plus-SO coupling splits each individual state of the uncoupled situation into two. The splitting in energy of ~0.112 eV of the resulting two peaks corresponds to the SO coupling of the atomic Cl plus the shift due to the electronic coupling as noted already. Examination of the time-dependent dynamics revealed a faster decay of the eigenstates in the coupled-state situation.

The photodetachment spectrum of ClD_2^- for a transition to the coupled manifold of ClD_2 electronic states is calculated and compared with the experimental results. This adds to our earlier work on the ClH_2^- photodetachment spectrum. The peak structure in the ClD_2^- detachment spectrum is more diffuse and broad compared to the ClH_2^- spectrum, in good accord with the experiment. The energetic separation between the observed peaks corresponds to the SO splitting of the atomic Cl. The transitions in ClD_2^- are much wider than in ClH_2^-, and the WP in the final SO states of the former samples more of the repulsive wall than the latter. The fine structures underneath each broad peak are quite complex, and the transition to all of the three SO states of the neutral contributes to this complexity.

In addition to the electronic and SO coupling, the Coriolis coupling terms of the Hamiltonian may also be important in the dynamics. The latter has been found to be crucial for some reactions occurring on a single electronic state.[38] Such a coupling is shown to have a relatively minor role in the F + H_2 reaction dynamics (see the second article of ref 32). An estimate of the effect of the Coriolis terms for Cl + H_2 would be valuable in order to assess the interplay of three different coupling mechanisms on its reaction dynamics. Such a study is presently being undertaken.

Acknowledgment. This study was supported in part by a research grant from the Council of Scientific and Industrial Research (grant 01(1917)/04/EMR -11), New Delhi. S. G. acknowledges the University Grants Commission (UGC), New Delhi, for a Junior Research Fellowship. The authors also thank UGC (the UPE program) and Department of Science and Technology (the High Performance Computational Facilities Program) for the computational facilities provided at the University of Hyderabad.

References and Notes

(1) Liu, K. *Annu. Rev. Phys. Chem*. **2001**, *52*, 139; *Int. Rev. Phys. Chem*. **2001**, *20*, 189. Casavecchia, P. *Rep. Prog. Phys*. **2000**, *63*, 355.

(2) Allison, T. C.; Mielke, S. L.; Schwenke, D. W.; Lynch, G. C.; Gordon, M. S.; Truhlar, D. G. In *Gas-phase reaction systems: experiments and models 100 years after Max Bodenstein*; Volp, H.-R., Wolfrum, J., Rannacher, R., Warnatz, J., Eds.; Springer: Heidelberg, 1996; p 111.

(3) Skouteris, D.; Manolopoulos, D. E.; Bian, W.; Werner, H.-J.; Lai, L.-H.; Liu, K. *Science* **1999**, *286*, 1713.

(4) Alexander, M. H.; Chapecchi, G.; Werner, H.-J. *Science*, **2002**, *296*, 715.

(5) Balucani, N.; Skouteris, D.; Cartechini, L.; Capozza, G.; Segoloni, E.; Casavecchia, P.; Alexander, M. H.; Chapecchi, G.; Werner, H.-J. *Phys. Rev. Lett*. **2003**, *91*, 013201.

(6) Schwenke, D. W.; Tucker, S. C.; Steckler, R.; Brown, F. B.; Lynch, G. C.; Trhular, D. G.; Garrett, B. C. *J. Chem. Phys*. **1989**, *90*, 3110.

(7) Allison, T. C.; Lynch, G. C.; Truhlar, D. G.; Gordon, M. S. *J. Phys. Chem*. **1996**, *100*, 13575.

(8) Bian, W.; Werner, H.-J. *J. Chem. Phys*. **2000**, *112*, 220.

(9) Yang, B.-H.; Gao, H.-T.; Han, K.-L.; Zhang, J. Z. H. *J. Chem. Phys*. **2000**, *113*, 1434.

(10) Capecchi, G.; Werner, H.-J. *Phys. Chem. Chem. Phys*. **2004**, *6*, 4975.

(11) Ghosal, S.; Mahapatra, S. *J. Chem. Phys*. **2004**, *121*, 5740.

(12) Ghosal, S.; Mahapatra, S. *Chem. Phys. Lett*. **2004**, *394*, 207.

(13) Alexander, M. H.; Capecchi, G.; Werner, H.-J. *Faraday Discuss*. **2004**, *127*, 59.

(14) Lee, S.-H.; Liu, K. *J. Chem. Phys*. **1999**, *111*, 6253.

(15) Dong, F.; Lee, S.-H.; Liu, K. *J. Chem. Phys*. **2001**, *115*, 1197.

(16) Ferguson, M. J.; Meloni, G.; Gomez, H.; Neumark, D. M. *J. Chem. Phys*. **2002**, *117*, 8181.

(17) Osterwalder, A.; Nee, M. J.; Zhou, J.; Neumark, D. M. *J. Chem. Phys*. **2004**, *121*, 6317.

(18) Wild, D. A.; Wilson, R. L.; Weiser, P. S.; Bieske, E. J. *J. Chem. Phys*. **2001**, *115*, 824.

(19) Balucani, N.; Skouteris, D.; Capozza, G.; Segoloni, E.; Casavecchia, P.; Alexander, M. H.; Capecchi, G.; Werner, H.-J. *Phys. Chem. Chem. Phys*. **2004**, *6*, 5007.

(20) Manolopolous, D. E.; Alexander, M. *Phys. Chem. Chem. Phys*. **2004**, *6*, 4984.

(21) Kosloff, R. *J. Phys. Chem*. **1988**, *92*, 2087. Balakrishnan, N.; Kalyanaraman, C.; Satyamurthy, N. *Phys. Rep*. **1997**, *280*, 79 and references therein. Nyman G.; Yu, H.-G. *Rep. Prog. Phys*. **2000**, *63*, 1001. Zhang, J. Z. H. In *Theory and Application of Quantum Molecular Dynamics*; World Scientific: Singapore, 1999.

(22) Heller, E. J. *Acc. Chem. Res*. **1981**, *14*, 368.

(23) We note an error in the definition of μ in refs 11 and 12. This error is purely typographical and does not affect the results presented in these articles.

(24) Rebentrost, F.; Lester, W. A., Jr. *J. Chem. Phys*. **1975**, *63*, 3737; **1976**, *64*, 3879; **1976**, *64*, 4223.

(25) Schatz, G. C.; McCabe, P.; Connor, J. N. L. *Faraday Discuss*. **1998**, *110*, 139. Whiteley, T. W. J.; Dobbyn, A. J.; Connor, J. N. L.; Schatz, G. C. *Phys. Chem. Chem. Phys*. **2000**, *2*, 549. Schatz, G. C.; Hankel, M.; Whiteley, T. W. J.; Connor, J. N. L. *J. Phys. Chem. A* **2003**, *107*, 7278.

(26) Alexander, M. H.; Werner, H.-J.; Manolopoulos, D. E. *J. Chem. Phys*. **1998**, *109*, 5710. Alexander, M. H.; Manolopoulos, D. E.; Werner, H.-J. *J. Chem. Phys*. **2000**, *113*, 11084.

(27) Köppel, H.; Domcke, W.; Cederbaum, L. S. *Adv. Chem. Phys*. **1984**, *57*, 59.

(28) Press, W. H.; Flannery, B. P.; Teukolsky, S. A.; Vatterling, W. T. *Numerical Recipes: The Art of Scientific Computing*; Cambridge University Press: Cambridge, U.K., 1986; p 125.

(29) Feit, M. D.; Fleck, J. A., Jr.; Steiger, A. *J. Comput. Phys*. **1982**, *47*, 412.

(30) Varandas, A. J. C.; Yu, H.-G. *Chem. Phys. Lett*. **1996**, *259*, 336.

(31) Mahapatra, S; Köppel, H. *J. Chem. Phys*. **1998**, *109*, 1721.

(32) Zhang, Y.; Xie, T.-X.; Han, K.-L. *J. Phys. Chem. A* **2003**, *107*, 10893. Zhang, Y.; Xie, T.-X.; Han, K.-L.; Zhang, J. Z. H. *J. Chem. Phys*. **2003**, *119*, 12921. Xie, T.-X.; Zhang, Y.; Zhao, M.-Y.; Han, K.-L. *Phys. Chem. Chem. Phys*. **2003**, *5*, 2034.

(33) Kosloff, D.; Kosloff, R. *J. Comput. Phys*. **1992**, *93*, 1982.

(34) Bačić, Z.; Light, J. C. *Annu. Rev. Phys. Chem*. **1989**, *40*, 469. Corey, G. C.; Lemoine, D. *J. Chem. Phys*. **1992**, *97*, 4115. Offer, A. R.; Balint-Kurti, G. G. *J. Chem. Phys*. **1994**, *101*, 10416.

(35) Engel, V. *Chem. Phys. Lett*. **1992**, *189*, 76. Manthe, U.; Meyer, H.-D.; Cederbaum, L. S. *J. Chem. Phys*. **1992**, *97*, 9062.

(36) Mahapatra, S; Sathyamurthy, N. *J. Chem. Soc., Faraday Trans*. **1997**, *93*, 773.

(37) Lepetit, B.; Peng, Z.; Kuppermann, A. *Chem. Phys. Lett*. **1990**, *166*, 572.

(38) Goldfield, E. M.; Meijer, A. J. H. M. *J. Chem. Phys*. **2000**, *113*, 11055. Carroll, T. E.; Goldfield, E. M. *J. Phys. Chem. A* **2001**, *105*, 2251. Sukiasyan, S.; Meyer, H.-D. *J. Chem. Phys*. **2002**, *116*, 10641.